

A Hybrid CNN-SVR for Airfoil Aerodynamic Coefficient Prediction

Sunarno^{1,2}, Aniati Murni Arymurthy¹

¹ Universitas Indonesia, Jl. Lingkar, Pondok Cina, Depok, 16424, Indonesia

² National Research and Innovation Agency, Republic of Indonesia

ARTICLE INFO

Article history:

Received May 24, 2024

Revised July 10, 2024

Published July 18, 2024

Keywords:

CNN;

SVR;

Aerodynamic Coefficient;

Airfoil;

Prediction

ABSTRACT

The prediction of aerodynamic coefficients on airfoils using machine learning is increasingly popular due to its efficiency in time and cost. Research typically focuses on a single image type without comparing various types and output quantities (single or multi-output). Although convolutional neural networks (CNN) are widely used, their final layer is often suboptimal as a linear operator, and feature extraction results contain many parameters that can still be trained. Support vector regression (SVR) with kernel functions effectively reduces common errors in feature vectors. We propose a hybrid method, AeroCNNSVR, combining CNN as a feature extractor and SVR as a regressor to predict aerodynamic coefficients on airfoils. This study focuses on the shape and position of airfoils according to the angle of attack (AoA) without considering flow conditions. Using 14533 aerodynamic coefficients from 563 airfoil types, we created a dataset of grayscale and RGB airfoil images. Results show the proposed method with grayscale images performs better because combining SVR strengthens the predictive model, while grayscale images accurately represent the airfoil's shape and position. AeroCNNSVR achieves lower RMSE values for C_l (0.101522), C_d (0.016450), and C_m (0.129661) compared to the CNN model's C_l (0.112493), C_d (0.019060), and C_m (0.130041). Additionally, AeroCNNSVR's R^2 values for C_l (0.976071), C_d (0.928700), and C_m (0.860574) surpass those of the CNN model (C_l 0.970620, C_d 0.904282, C_m 0.816355). This research contributes by 1) proposing an alternative besides CFD for predicting and identifying trends in aerodynamic coefficients of airfoils in a much shorter time during the design stage; 2) offering wind tunnel practitioners for early detection of configuration errors; 3) providing an overview of the aerodynamic characteristics of the airfoil under test, including the angle at which stall conditions occur.

This work is licensed under a [Creative Commons Attribution-Share Alike 4.0](https://creativecommons.org/licenses/by-sa/4.0/)



Corresponding Author:

Sunarno, Universitas Indonesia, Jl. Lingkar, Pondok Cina, Depok, 16424, Indonesia

Email: sunarno11@ui.ac.id

1. INTRODUCTION

The wing is a critical component of an aircraft [1], with the airfoil being its fundamental element [2], [3], [4]. The airfoil plays a pivotal role in determining both wing and overall aircraft performance [5], [6]. Achieving an optimal airfoil design involves aerodynamic studies using both experimental and numerical simulation approaches. Experimental methods entail testing airfoil models in wind tunnels to obtain and analyze aerodynamic characteristics. Wind tunnel testing involves all configurations; if results fail to meet expectations, iterative processes such as re-analysis, fabrication of new test models, and subsequent re-testing are initiated. Although the wind tunnel test results closely approximate real-world conditions, conducting these tests involved high costs, time, and resources [7], [8].

To reduce wind tunnel testing costs, numerical simulations using CFD are typically conducted as a preliminary step. CFD is employed to simulate airflow around test objects and determine their aerodynamic characteristics. Through CFD, it is anticipated that the test model prepared for wind tunnel testing will be matured, thereby reducing the frequency of model remanufacturing. Despite its advantages, CFD still requires extensive computational time and high computing resources [9]-[13]. Each simulation requires iterations to complete and involves high computational complexity per iteration [7], [14]. During the design phase, the speed of simulations is crucial for swift design analysis and evaluation to achieve optimal designs. This condition restricts simulations across all configurations due to time constraints and the computational demands per iteration [13]. Another critical aspect of using CFD involves the requirement for deep understanding and experience in physics and fluid mechanics [15].

Based on these conditions, together with the growth in aerodynamic testing and simulation data for airfoils, and advancements in machine learning, there has been increasing adoption of machine learning approaches for predicting aerodynamic coefficients on airfoils. This trend stems from machine learning's ability to produce accurate predictions in significantly shorter timeframes compared to experimental approaches or CFD simulations. Generally, the use of machine learning in predicting aerodynamic coefficients of airfoil models is categorized into two main approaches: parametric prediction and graphical prediction [8].

Parametric prediction utilizes multiple airfoil parameters to construct predictive models [16]-[20]. The aerodynamic parameters of an airfoil typically consist of three components: point coordinates, airfoil parameters, and flight conditions [21]. Esther *et al.*, 2020 [22] conducted research to predict the lift coefficient (Cl) and drag coefficient (Cd) using linear regression and support vector regression (SVR). This study employed three types of airfoils: NACA0012, RAE2822, and DPW Wing. The dataset encompassed variations in Mach number (0.1 - 0.9) and angle of attack (0° - 20°). Actual values of Cl and Cd as supervised data were obtained by conducting CFD on the three types of airfoils.

In 2021, Moin *et al.*, [21] utilized artificial neural networks (ANN) to forecast Cl, Cd, and pitching moment coefficient (Cm) for NACA 4-digit and 5-digit airfoils. The dataset included airfoil geometry coordinates at 5, 10, and 15 points, alongside flight conditions involving AoA (-10° to $+10^{\circ}$, incremented by 1°), Reynolds number (ranging from 100000 to 500000 with increments of 100000), and Mach number (ranging from 0.1 to 0.3 with increments of 0.1). Bhutara *et al.*, [23], also employed ANN in 2024 to predict Cl and Cd for NACA series 4 airfoils, using reference data for Cl and Cd obtained via the CFD solver XFLR5. The study involved 9 types of NACA4 airfoils, with variations in AoA (-5° to $+20^{\circ}$), chamber (0 to 2), chamber position (0 to 4), thickness (0.06 to 0.24), and Reynolds number (0.001e+06 to 50.0e+06).

In the study, airfoil parameters and flight conditions are considered influential in predicting Cl, Cd, and Cm. Determining parameters for this parametric prediction is challenging due to the difficulty in selecting the most influential parameters [8]. Additionally, the airfoil shape is represented by limited coordinates (x, y), and other parameters such as thickness, camber, and their positions are constrained. These limitations may lead to less accurate representation of the airfoil shape and position at specific AoA. The use of relatively uniform and limited airfoil types accelerates model training; however, increasing the dataset size would exponentially extend training time [8].

This condition has led many researchers to employ deep learning CNN for feature extraction from images in efforts to perform prediction and classification effectively [24]. Referred to as graphical prediction, this approach offers a solution to the limitations posed by previous parametric methods. The main advantage of this approach lies in its accurate ability to represent the shape and position of airfoils at various AoA. Furthermore, increasing the dataset size impacts training time linearly, unlike exponential impacts seen in parametric predictions [8]. The utilization of CNN for predicting airfoil aerodynamic coefficients was previously explored by Zhang *et al.* (2017) [15]. They employed a modified CNN LeNet-5, originally designed for document classification [25], to perform regression on the lift coefficient (Cl) of the airfoil. Actual lift coefficient data was obtained through CFD using XFOIL, based on predefined geometry data. This geometry data was used to generate grayscale airfoil images sized 49x49 pixels, with black representing the inner side of the airfoil and white the outer side. Mach number values were used to gradate the grayscale image according to Mach number variations. Since then, modified LeNet-5 models have been widely adopted for aerodynamic coefficient prediction, with adaptations including input conditioning using grayscale or RGB images, increasing the number of outputs from single to multi-output, and modifying the number of convolutional layers utilized.

Yuan *et al.* (2019) [26] employed the signed distance function (SDF) to generate RGB airfoil images sized at 32x32 pixels as input for a CNN model. The CNN architecture included 2 convolutional and pooling layers, followed by a fully connected layer prior to predicting the coefficients Cl, Cd, and Cm. Chen *et al.* (2020) [8] utilized a dataset comprising 300 airfoils to predict Cl, Cd, and Cm coefficients. Actual aerodynamic coefficient data were obtained through CFD simulations. Grayscale airfoil images sized at 85 x 85 pixels were

used, with the CNN architecture consisting of 2 convolutional and pooling layers using ReLU activation function, and a fully connected layer. The regression CNN employed MSE as its loss function, with RMSE utilized as the evaluation metric.

All mentioned studies employed a modified CNN LeNet-5 architecture, adapted from its original classification task to regression, focusing on one type of images, either on grayscale or RGB images, with various construction techniques, also focus on prediction results (single or multi-output). However, investigations into using modified LeNet-5 architectures as predictive models or integrating them with other methods for predicting airfoil aerodynamic coefficients have not been explored. In general, CNN has proven to perform well in feature extraction. However, the final layer of a CNN is considered a linear classification operator and may not always be the optimal choice, as the subsequent multi-layer perceptron (MLP) contains many parameters that can still be trained. On the other hand, SVM with kernel functions remains highly effective in minimizing general errors when applied to feature vectors [27]. Furthermore, combining CNN with SVM or CNN with SVR has proven to improve performance significantly compared to using CNN alone. Zhang *et al.* (2020) [27] proposed a hybrid CNN-SVR method for predicting gRNA. Khairandish *et al.* (2020) [28] proposed a hybrid CNN-SVM approach for tumor detection and MRI brain image classification. Ghimire *et al.* (2022) [29] developed a hybrid CNN-SVR model for solar radiation prediction. Rastegar *et al.* (2023) [30] applied a hybrid CNN-SVR approach to estimate blood pressure using ECG and PPG signals. Biswas, *et al.*, (2021) proposed a hybrid CNN-SVM for the classification of brain tumours [31]. Zhu, *et. al.*, using CNN-SVM for improved vehicle recognition [32]. Wenbing, *et. al.*, (2020) used hybrid CNN-SVR to predict the index measurement of wastewater [33].

Based on this issue, this research proposes a hybrid prediction model named AeroCNNSVR, which integrates CNN as feature extractors and Support Vector Regression (SVR) as regressors to predict the aerodynamic coefficients C_l , C_d , and C_m of an airfoil. The method utilizes alternating grayscale and RGB input images for model construction, with variations in convolutional layering and pooling aimed at optimizing model performance.

The research contributions in this research are: 1) proposing an alternative besides CFD for predicting and identifying trends in aerodynamic coefficients of airfoils in a much shorter time during the design stage; 2) offering wind tunnel practitioners for early detection of configuration errors; 3) providing an overview of the aerodynamic characteristics of the airfoil under test, including the angle at which stall conditions occur.

2. MATERIAL AND METHODS

The system proposed in this research is explained through the illustration in Fig. 1. In general, it consists of an input layer, a feature extraction layer, and a prediction layer. Model training employs the Mean Squared Error (MSE) loss function, while evaluation utilizes Root Mean Squared Error (RMSE) and R^2 . metrics.

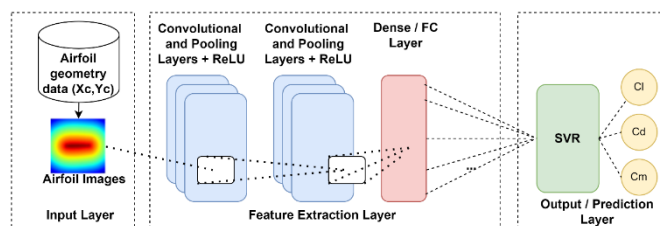


Fig. 1. System Architecture of Hybrid AeroCNNSVR

2.1. Airfoil

An airfoil is a fundamental component representing the cross-sectional shape of an aircraft wing, directly influencing wing and aircraft performance. It typically includes point coordinates, airfoil parameters, and flight conditions [21], [34], [35], as illustrated in Fig. 2. Airfoil nomenclature :

- Point Coordinates: (x,y) coordinates on the upper and lower surfaces forming the airfoil.
- Airfoil Parameters:
 - Leading Edge: The foremost point of the airfoil.
 - Trailing Edge: The rearmost point of the airfoil.
 - Mean Camber Line: The midpoint line between the upper and lower surfaces of the airfoil.
 - Cord Line (c): Straight line from the trailing edge to leading edge.
 - Camber: The maximum distance between mean camber line and chord line.
 - Camber Pos: The position of the chamber point is measured from the leading edge of the airfoil.
 - Thickness: Maximum distance between the upper and lower surfaces of an airfoil.

- Thickness Pos: The position of the thickness point is measured from the leading edge of the airfoil.
- Flight Conditions:
 - Angle of Attack (AOA): An angle between the relative wind and the chord line.
 - Reynold Number (Re)
 - Mach Number (Ma)

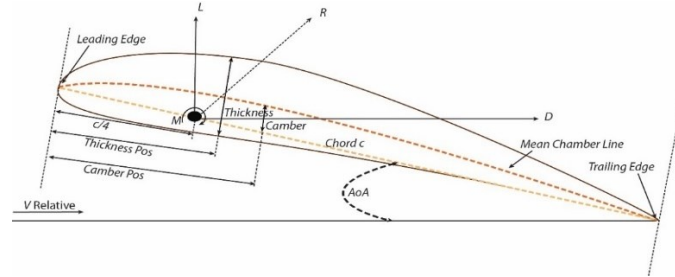


Fig. 2. Airfoil nomenclature

The airfoil shape is designed to make the airflow on the upper surface faster than the lower surface, creating a lower pressure on the upper surface. This pressure difference generates lift force (L), drag force (D), and pitching moment (M). The lift force acts perpendicular to the direction of the relative wind, while the drag force acts parallel to it. The pitching moment is caused by the airfoil's center of mass not being parallel to the centre of pressure. The forces and moments on the airfoil are generally expressed using the non-dimensional coefficients C_l , C_d , and C_m , as follows

$$C_l = \frac{L}{\frac{1}{2}\rho v^2 S} \quad (1)$$

where C_l is the lift coefficient, L is the lift force, ρ is the air density, v is the wind speed, and S is the surface area. In the context of a 2D airfoil, S is typically represented as the chord length (c). Thus, the equation becomes:

$$C_l = \frac{L}{\frac{1}{2}\rho v^2 c}, \quad C_d = \frac{D}{\frac{1}{2}\rho v^2 c}, \quad C_m = \frac{M}{\frac{1}{2}\rho v^2 c^2} \quad (2)$$

where c is the airfoil cord length, C_d is the drag coefficient, D is the drag force, C_m is the pitch moment coefficient, and M is the pitch moment

The airfoil design is developed to ensure laminar flow remains attached to its surface, resulting in a higher lift-to-drag ratio. Airfoil performance is commonly assessed by the C_l and C_d ratio [1], [36] - [39], as well as C_m [40]-[42].

2.2. Input Layer

Fig. 3. Preprocessing data on input layer, illustrates the data preprocessing procedure to obtain the dataset used as input for the prediction model.

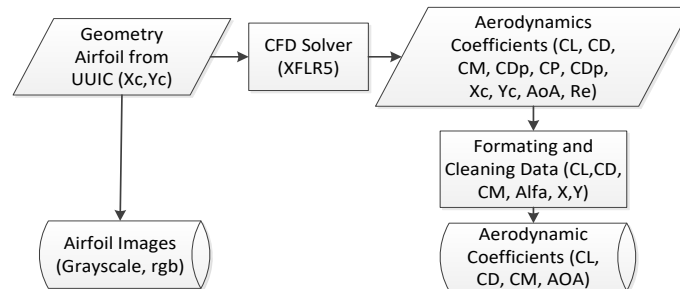


Fig. 3. Preprocessing data on input layer

2.2.1. Geometry Airfoil

The airfoil geometries were obtained from the UIUC Data Site (https://m-selig.ac.illinois.edu/ads/coord_database.html), comprising 574 airfoils. This dataset will be partitioned into training, validation, and testing sets in a ratio of 70:20:10. Each airfoil geometry entry stores non-dimensional coordinates (Xc, Yc), which will serve as inputs for CFD simulations and airfoil image generation.

2.2.2. CFD Solver

CFD was conducted on various airfoil types with AoA variations from -10^0 to $+20^0$, incremented by 1^0 . For flow conditions, $Ma = 0$ and $Re = 500000$ were utilized. The XFLR5 CFD solver was chosen due to its processing speed, comprehensive data output, and user-friendly interface [1], [43], [44]. Results obtained at this stage include C_l , C_d , C_m , CD_p values, coordinates (Xc and Yc), C_p , and XC_p . This research specifically focuses on C_l , C_d , and C_m values, as these coefficients directly represent airfoil performance, and by extension, aircraft performance. The CFD data serves as a reference (ground truth) for developing predictive models.

2.2.3. Formatting and Cleaning Data

The collected CFD data was reformatted to include only C_l , C_d , C_m , AOA, Xc, and Yc values. The data was structured in comma-separated values (CSV) files containing AOA, C_l , C_d , C_m , airfoil name, Re, Ma, and airfoil image name. At this stage, data points with fewer than 10 angles were removed to ensure dataset quality.

2.2.4. Airfoil Images

The airfoil images will be generated in grayscale and RGB formats based on the airfoil geometry (Xc, Yc). The chord length (c) is adjusted to fit the image size. In this study, the airfoil images are standardized to 128x128 pixels. Thus, the coordinates $X = Xc * c$ and $Y = Yc * c$ are determined. Grayscale image creation follows the procedure outlined in Fig. 4 at a 0^0 angle. Geometry data is transformed into X and Y coordinates by scaling with the chord length (128). Subsequently, these data are plotted using the *matplotlib library* with a black background. The airfoil position is centered within the frame, with coordinate axes removed and the inner airfoil filled with white color. Airfoil images are generated at angles ranging from -10^0 to $+20^0$ for each of the 574 airfoil types. The number of grayscale images produced for training is 9747, for validation is 3050, and for testing is 1462. The same quantities are generated for RGB airfoil images as well.

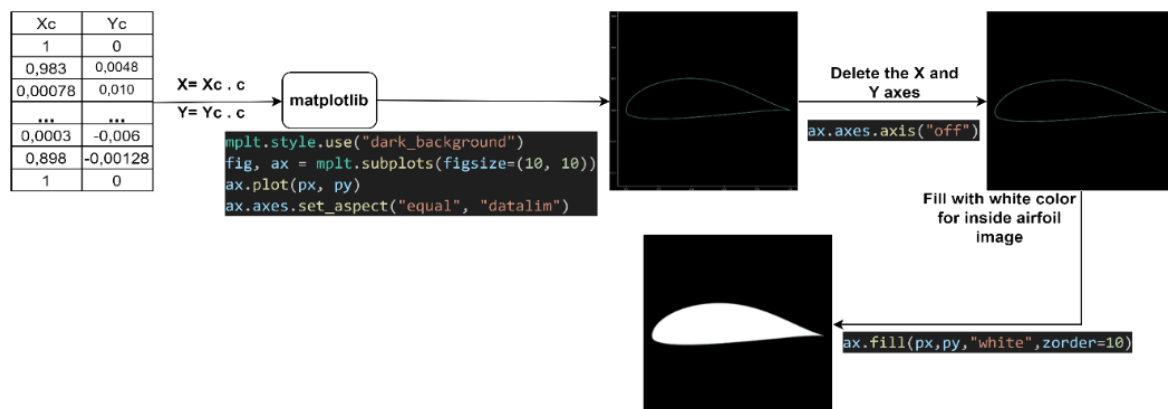


Fig. 4. Grayscale airfoil image conversion

The generation of RGB airfoil images follows the same principles as grayscale images, as depicted in Fig. 5. This process utilizes the *OpenCV library* for airfoil plotting, where the positive Y-axis points downward, necessitating inversion. And afterward, the airfoil's position is adjusted based on the G value to center it within the frame. The final step involves converting the image to RGB using the *scikit-fmm (skfmm) library*. This imaging enhances airfoil flexibility while maintaining consistent image shape across varying sizes.

For the results of airfoil image generation, please refer to Fig. 6 for grayscale images of airfoils A18sm, E423, E471, and NACA0021 at 0^0 degrees. Additionally, Fig. 7. presents RGB images of airfoils A18sm at 0^0 and $+20^0$, and NACA0021 at 0^0 and $+20^0$.

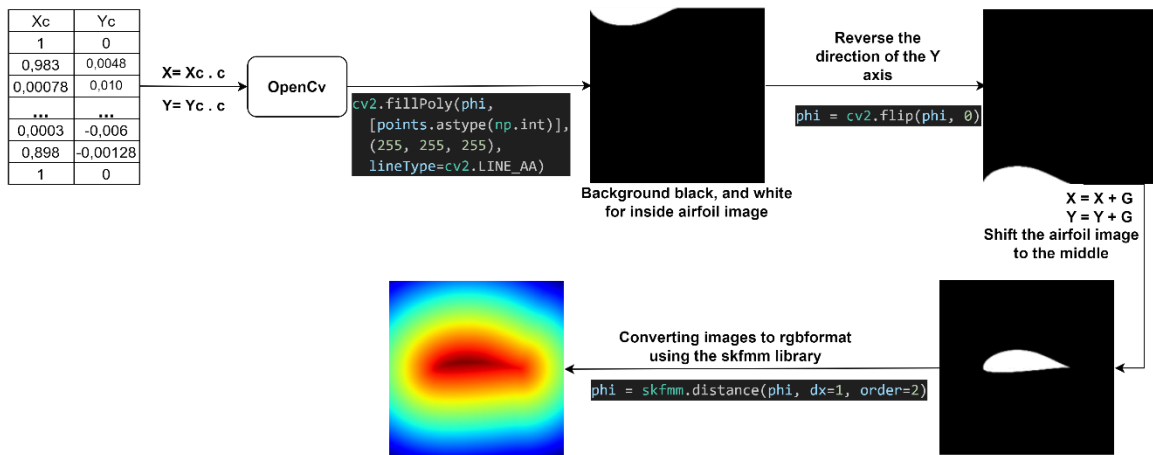


Fig. 5. Rgb airfoil image conversion

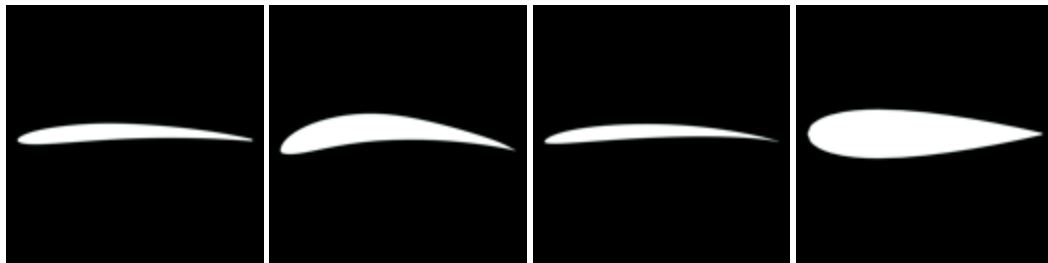


Fig. 6. Grayscale airfoil images

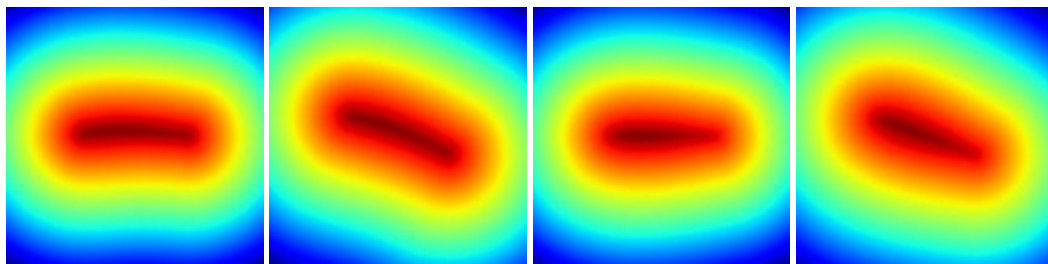


Fig. 7. Rgb airfoil images

2.3. Features Extraction Layer

At this stage, we constructed a CNN model based on a modified version of LeNet-5. The input airfoil images are of dimensions 128×128 pixels with 3 channels. The initial model employs 2 convolutional and pooling layers, as illustrated in Fig. 8. Each layer utilizes 16 filters/channels, using (3,3) kernels with a stride of 1 and a Rectified Linear Unit (ReLU) activation function, known for its effectiveness in producing better results [45]-[47]. The ReLU function will produce outputs zero if the input is less than zero and the input value itself if greater than or equal to zero [46], [48], [49]. Occurring after, variations of convolutional and pooling layers in the CNN models maintain a similar configuration, differing primarily in the number of filters/channels in each convolutional layer. As shown in Fig. 9 for the 3CL2FC model, Fig. 10 for the 4CL2FC model, and Fig. 11 for the 5CL2FC model, conv3 and conv4 use 64 filters, while conv5 in the 5CL2FC model uses 128 filters. Dense layers 1 (FC1) and 2 (FC2) are uniformly implemented across all models, using ReLU activation with 128 outputs for FC1 and linear activation with 3 outputs for FC2, representing the three aerodynamic coefficients.

The number of CNN models at this stage is 8 models consisting of 4 CNN models using grayscale airfoil image input data and 4 using RGB airfoil images. Each model will be trained and validated using a learning rate of 0.0001 with adaptive movement estimation (Adam) [50], [51] with an early stopping of 15 epochs to prevent overfitting.

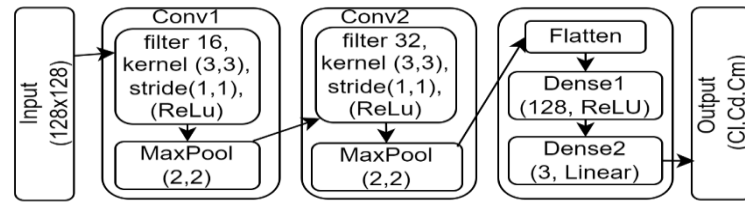


Fig. 8. CNN architecture 2CL2FC

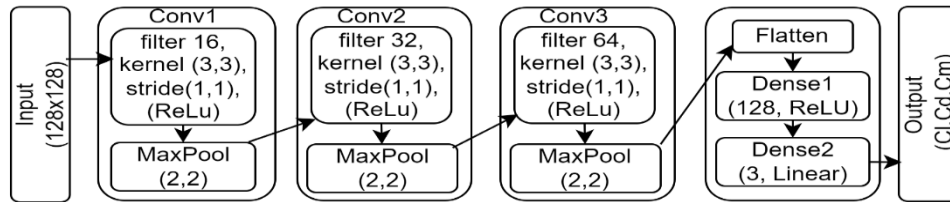


Fig. 9. CNN architecture 3CL2FC

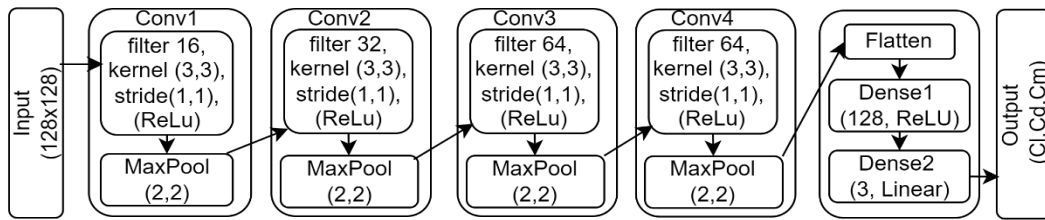


Fig. 10. CNN architecture 4CL2FC

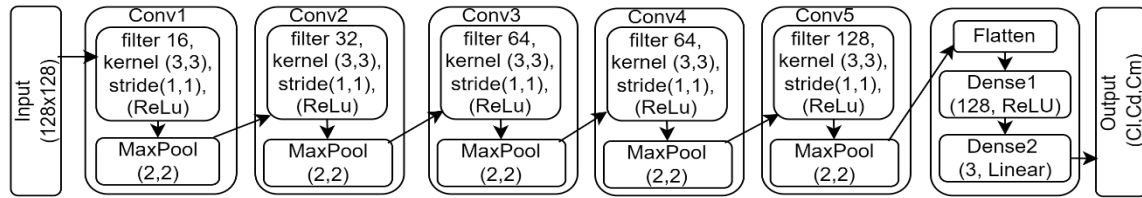


Fig. 11. CNN architecture 5CL2FC

2.4. Output / Prediction Layer

The previously trained CNN model will be pruned at its final layer (Dense2) and replaced with Support Vector Regression (SVR) to predict airfoil aerodynamic coefficients. SVR represents an upgraded version of the Support Vector Machine (SVM) suitable for regression tasks. SVM is a machine learning method that aims to find the best hyperplane that separates two classes with a maximum distance between the optimum hyperplane and separated hyperplane for each class (support vectors) as seen in Fig. 12. Initially a linear classifier, SVM evolved to handle non-linear problems by employing the kernel trick, which transforms input data into a higher-dimensional space (feature space) for separated linearly.

SVR is also developed based on the SVM principle, which involves mapping original data points from the input space into a higher-dimensional or even infinite-dimensional feature space to address regression problems [27], [29]. As illustrated in Fig. 13. SVR, epsilon (ϵ) is the distance between the hyperplane and the boundary that passes through the data point which is called the support vector. The margin ϵ is minimized to ensure all data points fit within a single distribution. This data distribution is formed to satisfy the regression function $f(x)$ of SVR, as follows:

$$f(x) = \langle w, x \rangle + b \quad (3)$$

where x is the input vector, w is the weight representing the hyperplane orientation, and b is the bias. Besides, the purpose of SVR is to minimize the following objective functions:

$$\min \left(\frac{1}{2} |w|^2 + C \sum_{i=1}^n (\xi_i + \xi_i^*) \right) \quad (4)$$

with limitations:

$$\begin{cases} y_i - \langle w, x_i \rangle - b \leq \epsilon + \xi_i \\ \langle w, x_i \rangle + b - y_i \leq \epsilon + \xi_i^* \\ \xi_i, \xi_i^* \geq 0 \end{cases} \quad (5)$$

where C is the regulatory parameter that regulates the trade-off between the complexity of the model and the penalty error, and ξ_i and ξ_i^* are the slack variables representing errors beyond the epsilon margin. Parameter tuning will be focused on during the training and validation of SVR in constructing the AeroCNNSVR model. The related parameters to be tuned include:

- The epsilon parameter (ϵ) determines the margin width in Support Vector Regression (SVR). A smaller epsilon value increases model sensitivity and improves performance on training data, although excessively small values can lead to overfitting. Conversely, larger values of epsilon may result in underfitting. In this study, epsilon values tested include 0.01, 0.1, 0.5, and 1.0.
- The regularization parameter (C) regulates the trade-off between minimizing errors and preventing overfitting in the model. A high C value reduces error but may lead to overfitting. The study varies C values as follows: 0.01, 0.1, 1, 10, and 100.
- The kernel type used in SVR training is varied across linear, polynomial, radial basis function (rbf), and sigmoid kernels.

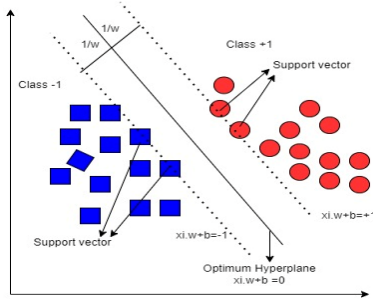


Fig. 12. SVM illustration

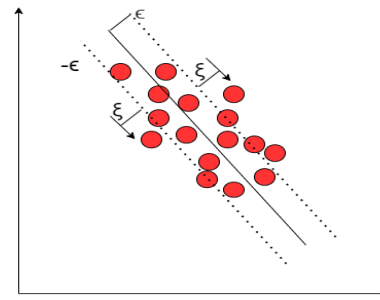


Fig. 13. SVR illustration

The combination of existing parameter values will be performed at the same time as the training model, in other words, the model will look for the composition of which parameters can produce the smallest loss. The model that has already been formed is the model with the best parameters. This method is more practical, although it increases model training time.

The loss function employed during model training and evaluation is Mean Square Error (MSE), consistent with previous research [8], [15], [26], indicating the model's performance quality. Evaluation metrics include Root Mean Square Error (RMSE) and Coefficient of Determination (R^2). RMSE involves squaring the difference between predicted and actual values, summing these squares, dividing by the number of data points, and taking the square root of the result. These metrics facilitate interpretable results aligned with actual data [52], [53]. R^2 explains the proportion of variance in the dependent variable explained by the independent variable. In this study, observed ground truth data (y_{gt}) serve as the independent variable, while predicted output (y_{pred}) acts as the dependent variable. R^2 ranges from 0 to 1, where values closer to 1 indicate less variance between y_{gt} and y_{pred} , which means the better [54].

Generally, the process conducted in the training, validation, and testing phases of the proposed method is outlined as follows:

- Collection of airfoil geometry data.
- Computational Fluid Dynamics (CFD) simulation of airfoil geometries to derive aerodynamic coefficients across a range of angles of attack (-10 to +20 degrees).
- Conversion and organization of CFD results into .csv format, encompassing coordinate data (x, y) for image creation and (Cl, Cd, Cm, angle) for labeling.
- Training and validation using Convolutional Neural Networks (CNN).
- Testing the CNN model using dedicated testing data.

6. Removal of the final dense layer (Dense2) from the CNN model and collect the results of the extraction feature.
7. Perform training and validation of SVR with input data from feature extraction before.
8. Evaluation of the AeroCNNSVR model performance using the same testing dataset employed in step 5.
9. Repetition of steps 4-7 for all model variations employing both grayscale and RGB input images.

3. RESULTS AND DISCUSSION

The training and validation processes will be performed on a CNN model used as the baseline, which will then be compared with the proposed model. The proposed model employs the same feature extraction method as the CNN model across various numbers of convolutional layers.

3.1. Training and Validation of CNN Model

The training history of CNN models with grayscale and RGB images is documented in Fig. 14 and Fig. 15. The training results indicate good performance (good fit) without overfitting. Initially, the MSE loss values on the training data are relatively higher compared to the validation data. By the 5th epoch, the MSE loss on the training data becomes lower than validation and remains stable for models 3CL2FC, 4CL2FC, and 5CL2FC. However, for the 2CL2FC model, the training MSE falls below validation at the 16th epoch. Consistent good fit and absence of overfitting are also evident in the training history of CNN models with RGB airfoil image inputs. Based on the number of epochs in both training histories, CNN models with RGB inputs require longer training times compared to grayscale, possibly due to the additional color-related information in RGB images. However, this study focuses on the shape and position of the airfoil based on AoA angle.

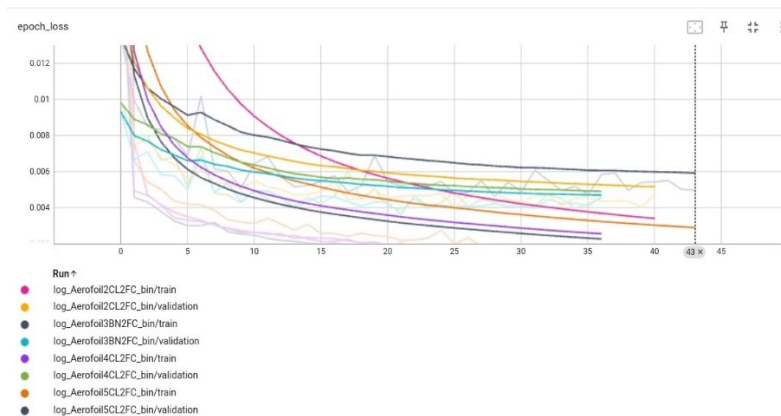


Fig. 14. Training history for CNN using grayscale airfoil images

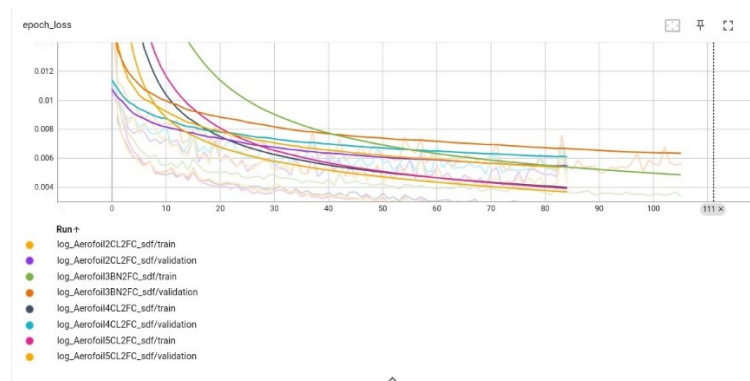


Fig. 15. Training history for CNN using rgb airfoil images

3.2. Experimental Result of CNN Model

The CNN model was tested using 1,462 airfoil images in the test dataset for each image type. Model performance was evaluated based on RMSE, R^2 , and graphical comparisons with actual data, detailed in Table 1 and Table 2. The results indicate that increasing the number of convolutional layers does not consistently enhance prediction model performance. The optimal CNN model for grayscale images was identified as

4CL2FC, featuring 4 convolutional layers with pooling and 2 dense layers. In contrast, for RGB images, CNN 5CL2FC demonstrated superior performance in RMSE and generally in R^2 , except for predicting C_m . When compared with both types of input images, grayscale images have better RMSE and R^2 scores than rgb for all model variations. This is because grayscale airfoil images represent the shape and the position of airfoil more clearly and accurately.

Table 1. Experimental Results of CNN Models using Grayscale Airfoil Images

No.	CNN Model	RMSE			R^2		
		Cl	Cd	C_m	Cl	Cd	C_m
1	2CL2FC	0.106522	0.022550	0.129322	0.973656	0.866019	0.799360
2	3CL2FC	0.101362	0.019157	0.128330	0.976146	0.903281	0.836036
3	4CL2FC	0.101148	0.016834	0.126865	0.976247	0.925333	0.805075
4	5CL2FC	0.114527	0.018812	0.131046	0.969548	0.906756	0.818049

Table 2. Experimental Results of CNN Models on RGB Airfoil Image

No.	CNN Model	RMSE			R^2		
		Cl	Cd	C_m	Cl	Cd	C_m
1	2CL2FC	0.118804	0.023139	0.131704	0.967231	0.858921	0.821047
2	3CL2FC	0.116313	0.023408	0.129724	0.968591	0.855623	0.819486
3	4CL2FC	0.119487	0.026536	0.140782	0.966853	0.814453	0.749404
4	5CL2FC	0.106127	0.019733	0.129605	0.973851	0.897395	0.780708

3.3. Experimental Result of AeroCNNSVR Model

The same testing data were utilized for the proposed AeroCNNSVR model. Prediction results are presented in Table 3 and Table 4, where the model achieving the overall RMSE and R^2 scores for predicting aerodynamic coefficients are 4CL2FC for grayscale data and 5CL2FC for RGB data. Metric evaluations consistently demonstrate that the grayscale data model outperforms across various configurations of convolutional and pooling layers. A comparison between CNN and AeroCNNSVR models reveals that the proposed model achieves superior RMSE and R^2 scores for each type of input image and across different convolutional layer configurations.

Table 3. Experimental Results of AeroCNNSVR Models on Grayscale Airfoil Images

No.	AeroCNNSVR Model	RMSE			R^2		
		Cl	Cd	C_m	Cl	Cd	C_m
1	2CL2FC	0.103302	0.018412	0.131251	0.975225	0.910677	0.842872
2	3CL2FC	0.105873	0.017792	0.130302	0.973976	0.916592	0.865359
3	4CL2FC	0.101522	0.016450	0.129661	0.976071	0.928700	0.860574
4	5CL2FC	0.109848	0.016692	0.130293	0.971985	0.926589	0.837078

Table 4. Experimental Results of AeroCNNSVR Models on RGB Airfoil Images

No.	AeroCNNSVR Model	RMSE			R^2		
		Cl	Cd	C_m	Cl	Cd	C_m
1	2CL2FC	0.120198	0.019793	0.129703	0.966458	0.896772	0.860302
2	3CL2FC	0.120198	0.019793	0.129703	0.966458	0.896772	0.860302
3	4CL2FC	0.112493	0.019060	0.130041	0.970620	0.904282	0.816355
4	5CL2FC	0.104297	0.018901	0.130502	0.974745	0.905867	0.865867

As seen in Fig. 16a, both the CNN and AeroCNNSVR models effectively predict Cl, following the actual data trend. However, at angles less than 5° degrees and post-stall, there are slight deviations between predicted and actual data. In Fig. 16b and Fig. 16c, for Cd and C_m predictions, AeroCNNSVR remains closer to the actual data trend compared to CNN, although not as effectively as in Cl predictions. Cd and C_m are relatively more challenging to predict due to their dependence on numerous and complex factors compared to Cl. Factors such as surface roughness, flow conditions around different airfoil shapes, changes in flow related to variations in angle of attack, and Reynold number will affect the pressure distribution in the airfoil surfaces which affects both Cd and C_m values. Small changes induced by these factors significantly impact variations in Cd and C_m . Meanwhile, Cl tends to correlate with total lift force, which is easier to predict, especially before a stall occurs.

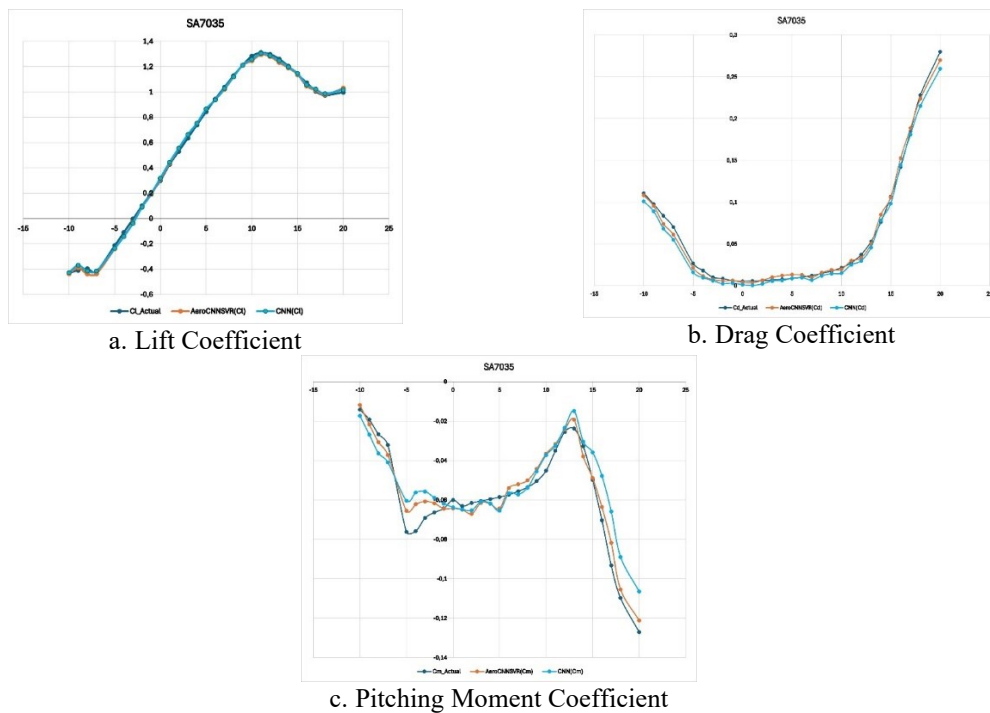


Fig. 16. Aerodynamic coefficient prediction from CNN and AeroCNNSVR

3.4. Discussion

Based on the training results in Table 1-Table 4, the addition of convolutional layers does not consistently improve the prediction model performance. Both the CNN and AeroCNNSVR models proposed show optimal performance in the 4CL2FC configuration, utilizing 4 convolutional layers. This suggests that in this model configuration, CNN consistently excels in recognizing airfoil shape and position features, yielding the best RMSE and R^2 values for predicting C_l , C_d , and C_m coefficients.

Table 1 and Table 3 show the RMSE and R^2 scores of the baseline CNN model compared to the AeroCNNSVR model using grayscale airfoil images. Across all model variations, the proposed model achieves superior evaluation scores compared to the CNN model. Similarly, in Table 2 and Table 4, the proposed RGB airfoil image model also outperforms the CNN model based on RMSE and R^2 scores. This improvement is due to the integration of SVR in the proposed method, which strengthens predictive capabilities beyond those achievable by CNN alone.

The type of airfoil image significantly influences the performance of prediction models. Grayscale images in all variations of CNN and the AeroCNNSVR model for predicting aerodynamic coefficients in this study yield superior RMSE and R^2 scores compared to models utilizing RGB airfoil images. Grayscale images provide clearer and more accurate depictions of the airfoil's shape and orientation at each Angle of Attack (AoA). Among the CNN prediction models using grayscale images, the CNN 4CL2FC model achieves the best performance with RMSE scores of C_l (0.112493), C_d (0.019060), C_m (0.130041), and corresponding R^2 scores of C_l (0.970620), C_d (0.904282), C_m (0.816355). Similarly, in the AeroCNNSVR model, the 4CL2FC model demonstrates RMSE scores for C_l (0.101522), C_d (0.016450), C_m (0.129661), and R^2 scores for C_l (0.976071), C_d (0.928700), C_m (0.860574).

Both CNN and AeroCNNSVR models can predict the C_l coefficient quite accurately. Especially at angles above -5° and up to the stall, as seen in Fig. 16a. The proposed method can produce prediction results that are closer to the actual data than the baseline CNN model. As seen in Fig. 16b. and Fig. 16c, where the predicted data trend of the proposed method is closer to the actual data trend for the predicted coefficients C_d and C_m .

4. CONCLUSION

The research focuses on the shape of the airfoil based on the geometry of the Airfoil and its position based on an AoA. The type of airfoil image significantly impacts the predictive model's performance and training speed. The grayscale airfoil image in this study was able to produce better performance than the rgb image because the grayscale airfoil images represent the shape and the position of airfoil more clearly and accurately. Grayscale airfoil images also make the model train faster because they are simpler than RGB images. The CNN

and AeroCNNSVR architectures explored in this study vary in layer depth, specifically 2CL2FC, 3CL2FC, 4CL2FC, and 5CL2FC configurations. The proposed models consistently achieve better RMSE and R2 scores across all variations. The highest performance is observed with the AeroCNNSVR architecture using 4CL2FC on grayscale airfoil images, yielding RMSE scores of Cl (0.101522), Cd (0.016450), Cm (0.129661), and R2 scores of Cl (0.976071), Cd (0.928700), Cm (0.860574). The CNN and AeroCNNSVR models consistently perform best with the 4CL2FC configuration, which shows the consistency of the feature extraction done by CNN. And by combining with SVR, the predictions obtained become stronger. Prediction graphs for the SA7035 airfoil demonstrate that predicted data trends closely follow actual data trends. This method offers an alternative perspective for predicting airfoil aerodynamic coefficients, providing rapid predictive capabilities useful for wind tunnel testing to assess aerodynamic characteristics. The models accommodate diverse airfoil shapes encountered in real-world designs, facilitating accurate predictions across varying airfoil types.

In this study, CFD data that is empty or has fewer than 10 angles for an airfoil will not be used as part of the dataset. Future research can address this by increasing the number of data points during the CFD process, ensuring aerodynamic coefficients are obtained at all desired angles of attack. Additionally, other factors such as flow conditions can be examined further, as this study primarily focuses on the shape and position of the airfoil based on geometry and angle of attack to improve predictions, particularly for the drag coefficient (Cd) and pitching moment (Cm). There is also potential to investigate the impact of different input image sizes on the model. Smaller airfoil images tend to be blurry, while larger images can strain the model training process. For aircraft wing testing, the proposed hybrid AeroCNNSVR method can be used to predict the aerodynamic coefficients of aircraft wings.

REFERENCES

- [1] K. K. Chaitanyaa, C. R. Patil, B. Pal, and D. Dandotiya, "Aerodynamic Analysis and Optimization of Airfoils Using Vortex Lattice Method," in *IOP Conference Series: Materials Science and Engineering*, vol. 1013, no. 1, p. 012023, Jan. 2021. <https://doi.org/10.1088/1757-899X/1013/1/012023>.
- [2] Y. Wang, K. Shimada, and A. Barati Farimani, "Airfoil GAN: encoding and synthesizing airfoils for aerodynamic shape optimization," *J Comput Des Eng*, vol. 10, no. 4, pp. 1350 – 1362, 2023, <https://doi.org/10.1093/jcde/qwad046>.
- [3] D. A. Masters, N. J. Taylor, T. C. S. Rendall, C. B. Allen, and D. J. Poole, "A Geometric Comparison of Airfoil Shape Parameterisation Methods," *AIAA journal*, vol. 55, no. 5, pp. 1575-1589, 2017, <https://doi.org/10.2514/1.J054943>.
- [4] J. D. Hoyos, C. Echavarría, J. P. Alvarado, G. Suárez, J. A. Niño, and J. I. García, "Two-Way Coupled Aero-Structural Optimization of Stable Flying Wings," *Aerospace*, vol. 10, no. 4, Apr. 2023, <https://doi.org/10.3390/aerospace10040346>.
- [5] J. Yi and F. Deng, "Cooperation of Thin-Airfoil Theory and Deep Learning for a Compact Airfoil Shape Parameterization," *Aerospace*, vol. 10, no. 7, Jul. 2023, <https://doi.org/10.3390/aerospace10070650>.
- [6] H. Hares and G. Mebarki, "Influence of Wing Shape on Airfoil Performance: a Comparative Study," *WSEAS Transactions on Fluid Mechanics*, vol. 18, pp. 49–57, 2023, <https://doi.org/10.37394/232013.2023.18.5>.
- [7] Y. Wang *et al.*, "An Intelligent Method for Predicting the Pressure Coefficient Curve of Airfoil-Based Conditional Generative Adversarial Networks," *IEEE Trans Neural Netw Learn Syst*, vol. 34, no. 7, pp. 3538–3552, Jul. 2023, <https://doi.org/10.1109/TNNLS.2021.3111911>.
- [8] H. Chen, L. He, W. Qian, and S. Wang, "Multiple aerodynamic coefficient prediction of airfoils using a convolutional neural network," *Symmetry (Basel)*, vol. 12, no. 4, Apr. 2020, <https://doi.org/10.3390/SYM12040544>.
- [9] E. A. -Pérez, "Data mining and machine learning techniques for aerodynamic databases: Introduction, methodology and potential benefits," *Energies (Basel)*, vol. 13, no. 21, Nov. 2020, <https://doi.org/10.3390/en13215807>.
- [10] H. Chen, L. He, W. Qian, and S. Wang, "Multiple Aerodynamic Coefficient Prediction of Airfoils Using a Convolutional Neural Network," *Symmetry (Basel)*, vol. 12, no. 4, 2020, <https://doi.org/10.3390/sym12040544>.
- [11] C. Lozano, "Surrogate modelling for aerodynamic coefficients prediction in aeronautical configurations," In *Proceedings of the 8th European Conference for Aeronautics and Space Sciences (EUCASS)*, pp. 1-4, 2019, <https://doi.org/10.13009/EUCASS2019-870>.
- [12] J. Tao and G. Sun, "Application of deep learning based multi-fidelity surrogate model to robust aerodynamic design optimization," *Aerosp Sci Technol*, vol. 92, pp. 722–737, Sep. 2019, <https://doi.org/10.1016/j.ast.2019.07.002>.
- [13] K. Balla, R. Sevilla, O. Hassan, and K. Morgan, "An application of neural networks to the prediction of aerodynamic coefficients of aerofoils and wings," *Appl Math Model*, vol. 96, pp. 456–479, Aug. 2021, <https://doi.org/10.1016/j.apm.2021.03.019>.
- [14] X. Hui, J. Bai, H. Wang, and Y. Zhang, "Fast pressure distribution prediction of airfoils using deep learning," *Aerosp Sci Technol*, vol. 105, Oct. 2020, <https://doi.org/10.1016/j.ast.2020.105949>.
- [15] Y. Zhang, W.-J. Sung, and D. Mavris, "Application of Convolutional Neural Network to Predict Airfoil Lift Coefficient," In *2018 AIAA/ASCE/AHS/ASC structures, structural dynamics, and materials conference*, p. 1903, Dec. 2017, [Online]. <http://arxiv.org/abs/1712.10082>
- [16] W. Peng, Y. Zhang, E. Laurendeau, and M. C. Desmarais, "Learning aerodynamics with neural network," *Sci Rep*, vol. 12, no. 1, Dec. 2022, <https://doi.org/10.1038/s41598-022-10737-4>.

- [17] Z. Ti, X. W. Deng, and H. Yang, "Wake modeling of wind turbines using machine learning," *Appl Energy*, vol. 257, Jan. 2020, <https://doi.org/10.1016/j.apenergy.2019.114025>.
- [18] B. N. Hanna, N. T. Dinh, R. W. Youngblood, and I. A. Bolotnov, "Machine-learning based error prediction approach for coarse-grid Computational Fluid Dynamics (CG-CFD)," *Progress in Nuclear Energy*, vol. 118, Jan. 2020, <https://doi.org/10.1016/j.pnucene.2019.103140>.
- [19] A. Teimourian, D. Rohacs, K. Dimililer, H. Teimourian, M. Yildiz, and U. Kale, "Airfoil aerodynamic performance prediction using machine learning and surrogate modeling," *Heliyon*, vol. 10, no. 8, Apr. 2024, <https://doi.org/10.1016/j.heliyon.2024.e29377>.
- [20] C. Liu, X. Wang, and X. Liu, "Prediction of aircraft aerodynamic coefficient based on data-driven method," in *Journal of Physics: Conference Series*, vol. 2024, no. 1, p. 012039, Sep. 2021, <https://doi.org/10.1088/1742-6596/2024/1/012039>.
- [21] H. Moin, H. Z. I. Khan, S. Mobeen, and J. Riaz, "Airfoil's Aerodynamic Coefficients Prediction using Artificial Neural Network," In *2022 19th International Bhurban Conference on Applied Sciences and Technology (IBCAST)*, pp. 175-182, Sep. 2021, <https://doi.org/10.1109/IBCAST54850.2022.9990112>.
- [22] E. A. -Pérez, "Data mining and machine learning techniques for aerodynamic databases: Introduction, methodology and potential benefits," *Energies (Basel)*, vol. 13, no. 21, Nov. 2020, <https://doi.org/10.3390/en13215807>.
- [23] H. Bhutra, K. Chandan, and T. V. Smitha, "Effective Prediction of Coefficients and Performance of Airfoil Using ANN," in *2024 4th International Conference on Advances in Electrical, Computing, Communication and Sustainable Technologies, ICAECT 2024*, pp. 1-5, 2024. <https://doi.org/10.1109/ICAECT60202.2024.10469032>.
- [24] I. L. Jernelv, D. R. Hjelme, Y. Matsuura, and A. Aksnes, "Convolutional neural networks for classification and regression analysis of one-dimensional spectral data," *arXiv preprint arXiv:2005.07530*, May 2020, [Online]. <http://arxiv.org/abs/2005.07530>
- [25] Y. Lecun, L. Eon Bottou, Y. Bengio, and P. H. Haffner, "Gradient-Based Learning Applied to Document Recognition," *Proceedings of the IEEE*, vol. 86, no. 11, pp. 2278-2324, 1998, <https://doi.org/10.1109/5.726791>.
- [26] Z. Yuan, Y. Wang, Y. Qiu, J. Bai, and G. Chen, "Aerodynamic Coefficient Prediction of Airfoils with Convolutional Neural Network," in *Lecture Notes in Electrical Engineering*, pp. 34-46, 2019, https://doi.org/10.1007/978-981-13-3305-7_3.
- [27] G. Zhang, Z. Dai, and X. Dai, "A Novel Hybrid CNN-SVR for CRISPR/Cas9 Guide RNA Activity Prediction," *Front Genet*, vol. 10, Jan. 2020, <https://doi.org/10.3389/fgene.2019.01303>.
- [28] M. O. Khairandish, M. Sharma, V. Jain, J. M. Chatterjee, and N. Z. Jhanjhi, "A Hybrid CNN-SVM Threshold Segmentation Approach for Tumor Detection and Classification of MRI Brain Images," *IRBM*, vol. 43, no. 4, pp. 290-299, Aug. 2022, <https://doi.org/10.1016/j.irbm.2021.06.003>.
- [29] S. Ghimire, B. Bhandari, D. C. -Pérez, R. C. Deo, and S. S. -Sanz, "Hybrid deep CNN-SVR algorithm for solar radiation prediction problems in Queensland, Australia," *Eng Appl Artif Intell*, vol. 112, Jun. 2022, <https://doi.org/10.1016/j.engappai.2022.104860>.
- [30] S. Rastegar, H. Gholam Hosseini, and A. Lowe, "Hybrid CNN-SVR Blood Pressure Estimation Model Using ECG and PPG Signals," *Sensors*, vol. 23, no. 3, Feb. 2023, <https://doi.org/10.3390/s23031259>.
- [31] A. Biswas and M. S. Islam, "Hybrid CNN-SVM Model for Brain Tumor Classification utilizing Different Datasets," in *Proceedings of International Conference on Electronics, Communications and Information Technology, ICECIT 2021*, pp. 1-4, 2021, <https://doi.org/10.1109/ICECIT54077.2021.9641201>.
- [32] J. Zhu, Y. Ju, and M. Xia, "Vehicle recognition model based on improved CNN-SVM," in *Proceedings - 2021 2nd International Seminar on Artificial Intelligence, Networking and Information Technology, AINIT 2021*, pp. 294-297, 2021, <https://doi.org/10.1109/AINIT54228.2021.00065>.
- [33] W. Fan and Z. Zhang, "A CNN-SVR Hybrid Prediction Model for Wastewater Index Measurement," in *Proceedings - 2020 2nd International Conference on Advances in Computer Technology, Information Science and Communications, CTISC 2020*, pp. 90-94, Mar. 2020, <https://doi.org/10.1109/CTISC49998.2020.00022>.
- [34] Mohammad Erfan Khodabakhshi and Masoud Aryanpour, "Numerical Solution of Inviscid and Viscous Flow Across NACA0010 Airfoil with different Angles of Attack," *Int J Sci Res Sci Eng Technol*, pp. 268-279, Aug. 2023, <https://doi.org/10.32628/ijrsret23103211>.
- [35] A. Kulshreshtha, S. K. Gupta, and P. Singhal, "FEM/CFD analysis of wings at different angle of attack," in *Materials Today: Proceedings*, pp. 1638-1643, 2019, <https://doi.org/10.1016/j.matpr.2020.02.342>.
- [36] O. A. Zargar *et al.*, "The effects of surface modification on aerodynamic characteristics of airfoil DU 06 W 200 at low Reynolds numbers," *International Journal of Thermofluids*, vol. 16, Nov. 2022, <https://doi.org/10.1016/j.ijft.2022.100208>.
- [37] F. L. Rashid, H. S. Abd, and E. Q. Hussein, "Numerical study of the air flow over modified NACA 2412 airfoil using CFD," in *AIP Conference Proceedings*, vol. 2415, no. 1, Dec. 2022, <https://doi.org/10.1063/5.0092303>.
- [38] J. Hoyos, J. H. Jiménez, C. Echavarría, and J. P. Alvarado, "Airfoil Shape Optimization: Comparative Study of Meta-heuristic Algorithms, Airfoil Parameterization Methods and Reynolds Number Impact," *IOP Conf Ser Mater Sci Eng*, vol. 1154, no. 1, p. 012016, Jun. 2021, <https://doi.org/10.1088/1757-899x/1154/1/012016>.
- [39] H. Hares and G. Mebarki, "Influence of Wing Shape on Airfoil Performance: a Comparative Study," *WSEAS Transactions on Fluid Mechanics*, vol. 18, pp. 49-57, 2023, <https://doi.org/10.37394/232013.2023.18.5>.
- [40] R. Balaşa, C. C. Andrei, A. G. Andrei, and A. Semenescu, "the impact of different outward and inward protrusion positions on the NACA 1410 airfoil section at various angles of attack," *Mechanical Testing and Diagnosis*, vol. 11, no. 2, pp. 10-17, Jul. 2021, <https://doi.org/10.35219/mtd.2021.2.02>.

- [41] Y. Sowmyashree *et al.*, "Study on effect of semi-circular dimple on aerodynamic characteristics of NACA 2412 airfoil," in *AIP Conference Proceedings*, vol. 2204, no. 1, Jan. 2020, <https://doi.org/10.1063/1.5141572>.
- [42] M. T. Islam, A. M. E. Arefin, M. H. Masud, and M. Mourshed, "The effect of Reynolds number on the performance of a modified NACA 2412 airfoil," in *AIP Conference Proceedings*, vol. 1980, no. 1, Jul. 2018. <https://doi.org/10.1063/1.5044325>.
- [43] F. Rahman, S. Wasim, and U. Huda, "Numerical Analysis of Modified NACA 4412 Airfoil for Implementation of Low Reynolds Numbers VAWTs," *Journal of Mechanical Engineering*, vol. ME X7, no. 1, 2022. [Online]. <https://www.researchgate.net/publication/380099778>
- [44] F. Akter, M. A. Hoque, K. A. Ekram, B. Saha, and M. J. Hasan, "Design of a Novel Aerofoil of a Light Aircraft for Robust Aerodynamic Performance at High Reynolds Number Regime Using XFLR5," *Arab J Sci Eng*, pp. 1-17, 2024, <https://doi.org/10.1007/s13369-024-08837-6>.
- [45] A. K. Dubey and V. Jain, "Comparative Study of Convolution Neural Network's Relu and Leaky-Relu Activation Functions," In *Applications of Computing, Automation and Wireless Systems in Electrical Engineering: Proceedings of MARC 2018*, pp. 873–880, 2019, https://doi.org/10.1007/978-981-13-6772-4_76.
- [46] X. Jiang, Y. Pang, X. Li, J. Pan, and Y. Xie, "Deep neural networks with Elastic Rectified Linear Units for object recognition," *Neurocomputing*, vol. 275, pp. 1132–1139, Jan. 2018, <https://doi.org/10.1016/j.neucom.2017.09.056>.
- [47] S. R. Dubey, S. K. Singh, and B. B. Chaudhuri, "Activation functions in deep learning: A comprehensive survey and benchmark," *Neurocomputing*, vol. 503, pp. 92–108, Sep. 2022. <https://doi.org/10.1016/j.neucom.2022.06.111>.
- [48] M. Tanaka, "Weighted Sigmoid Gate Unit for an Activation Function of Deep Neural Network," *Pattern Recognition Letters*, vol. 135, pp. 354-359, Oct. 2018, [Online]. <http://arxiv.org/abs/1810.01829>.
- [49] A. M. Javid, S. Das, M. Skoglund, and S. Chatterjee, "A ReLU Dense Layer to Improve the Performance of Neural Networks," In *ICASSP 2021-2021 IEEE International Conference on Acoustics, Speech and Signal Processing (ICASSP)*, pp. 2810-2814, Oct. 2020, [Online]. Available: <http://arxiv.org/abs/2010.13572>.
- [50] K. Bae, H. Ryu, and H. Shin, "Does Adam optimizer keep close to the optimal point?," *arXiv preprint arXiv:1911.00289*, Nov. 2019, [Online]. <http://arxiv.org/abs/1911.00289>.
- [51] S. Bock and M. Weiß, "A Proof of Local Convergence for the Adam Optimizer," In *2019 international joint conference on neural networks (IJCNN)*, pp. 1-8, 2019, <https://doi.org/10.1109/IJCNN.2019.8852239>.
- [52] K. A. Beyene, "Comparative study of linear and quadratic model equations for prediction and evaluation of surface roughness of a plain-woven fabric," *Research Journal of Textile and Apparel*, vol. 27, no. 2, pp. 281–298, May 2023, <https://doi.org/10.1108/RJTA-08-2021-0107>.
- [53] A. Gautama Putrada, N. Alamsyah, I. D. Oktaviani, and M. N. Fauzan, "A Hybrid Genetic Algorithm-Random Forest Regression Method for Optimum Driver Selection in Online Food Delivery," *Jurnal Ilmiah Teknik Elektro Komputer dan Informatika (JITEKI)*, vol. 9, no. 4, pp. 1060–1079, 2023, <https://doi.org/10.26555/jiteki.v9i4.27014>.
- [54] A. Gautama Putrada, N. Alamsyah, I. D. Oktaviani, and M. N. Fauzan, "A Hybrid Genetic Algorithm-Random Forest Regression Method for Optimum Driver Selection in Online Food Delivery," *Jurnal Ilmiah Teknik Elektro Komputer dan Informatika (JITEKI)*, vol. 9, no. 4, pp. 1060–1079, 2023, <https://doi.org/10.26555/jiteki.v9i4.27014>.

BIOGRAPHY OF AUTHORS



Sunarno is pursuing a postgraduate's degree in Magister of Computer Science an Universitas Indonesia. He works at National Research and Innovation Agency in Aerodynamics, Aeroelastic and Aeroacoustics Laboratory. Email: sunarno11@ui.ac.id. Orcid: <https://orcid.org/0009-0000-2069-6496>.



Aniati Murni Arymurthy is a professor and researcher at Faculty of Computer Science, Universitas Indonesia. Her research interests are Pattern Recognition, Image Processing, and Spatial Data. Email: aniati@cs.ui.ac.id. Orcid: <https://orcid.org/0000-0002-2762-7001>.